Journal Name

ARTICLE

Site controlled Red-Yellow-Green light emitting InGaN Quantum Discs on nano-tipped GaN rods

Received 00th January 20xx,
Accepted 00th January 20xx

DOI: 10.1039/x0xx00000x

www.rsc.org/

M. Conroy*[a,b,c,d], H. Li[a,b], G. Kusch[e], C. Zhao[f], B. Ooi[f], P. R. Edwards[e], R. W. Martin[e], J. D. Holmes[a,c,d], P. J. Parbrook*[a,b]

We report a method of growing site controlled InGaN multiple quantum discs (QDs) at uniform wafer scale on coalescence free ultra-high density (>80%) nanorod templates by metal organic chemical vapour deposition (MOCVD). The dislocation and coalescence free nature of the GaN space filling nanorod arrays eliminates the well-known emission problems seen in InGaN based visible light sources that these types of crystallographic defects cause. Correlative scanning transmission electron microscopy (STEM), energy-dispersive x-ray (EDX) mapping and cathodoluminescence (CL) hyperspectral imaging illustrates the controlled site selection of the red, yellow and green (RYG) emission at these nano tips. This article reveals that the nanorod tips' broad emission in the RYG visible range is in fact achieved by manipulating the InGaN QD's confinement dimensions, rather than significantly increasing the In%. This article details the easily controlled method of manipulating the QDs dimensions producing high crystal quality InGaN without complicated growth conditions needed for strain relaxation and alloy compositional changes seen for bulk planar GaN templates.

Introduction

InGaN based semiconductor optoelectronic devices are leading the way in the evolution of broad spectrum solid state lighting.[1-4] Their potential wavelength emission can in theory produce light across the entire visible spectrum simply by alloying In% in the InGaN active region.[5] Although light emitting diodes (LEDs) promise a high degree of functionality and performance, there are still improvements required to reach the longer wavelengths beyond blue emission. Growing InGaN multiple quantum wells (MQWs) with sufficient In% to emit light above 520 nm has been difficult due to the crystallographic defects formed, better known as the "green gap".[6] As InGaN grown on GaN increases in thickness there is a huge stress caused by the lattice mismatch.[7] The main stress relieving mechanisms possible for epitaxially grown InGaN on planar layers is through dislocation formation[8-9] which are known to have a significant impact on the internal quantum efficiency.[10] GaN nanorods used as the template for InGaN MQW growth provide a strain free surface without dislocations due to the large surface-to-volume ratio of III-N nanorods.[11-13] These dislocation free GaN nanostructures are also reported to increase light extraction efficiency and enlarge the light emitting surface.[14-16] Additionally moving from bulk to nanoscale provides many new optical properties[17-18] bridging the green gap.

Until recently GaN nanorods were mainly produced by bottom up growth methods such as spontaneous self-assembly molecular beam epitaxy[19], vapor liquid solid[20-21] and selective area growth.[10] Although these methods can produce high crystal quality GaN with negligible extended defect content, their spontaneous origin causes increasingly large areas of coalescence to be formed with increasing density.[22] At these coalesced nanorod regions the mutual misorientation results in extended defects such as basal plane stacking faults and dislocations when the strain cannot be accommodated elastically.[23-25] The increased strain caused by the coalescence has a significant impact on the optical properties of the nanorod LEDs: as reported by several groups the PL peaks broaden greatly with increasing fill factor.[19, 26-28] Furthermore, additional peaks associated with basal stacking faults[25, 29] and threading dislocations[30] only begin to appear above a certain fill factor. To overcome these issues a new two-step top down/bottom up method has started to be used for high crystal quality GaN nanorods.[31-35]

The two-step method allows for the combined benefits from planar crystal growth such as low impurity incorporation and controlled doping; and nanorod architecture benefits such as low dislocation density and strain. Additionally this method avoids coalescence by spacing out the nanorods in an organized pattern thus lowering the density of rods significantly. However high fill factor/density is an essential aspect for GaN nanorod LEDs to decrease the required current density in the junction at constant total currents.[36] Using a modified space filling growth model as we reported previously for AlN elsewhere,[37] InGaN active regions can now be grown on highly dense (>80%) arrays avoiding the issue of coalescing rods.

[a] Tyndall National Institute, Dyke Parade, Cork City, Ireland. Email: michele.conroy@pnnl.gov, peter.parbrook@tyndall.ie
[b] School of Engineering, University College Cork, Cork City, Ireland
[c] Department of Chemistry, University College Cork, Cork City, Ireland
[d] AMBER@CRANN, Trinity College Dublin, Dublin City, Ireland
[e] Department of Physics, SUPA, University of Strathclyde, 107 Rottenrow, Glasgow G4 0NG, U.K.
[f] Photonics Laboratory, King Abdullah University of Science and Technology (KAUST), Thuwal 23955-6900, Saudi Arabia
†Electronic Supplementary Information (ESI) available see DOI: 10.1039/x0xx00000x

In this article we measure by CL hyperspectral a red shift of >100 nm at the c-plane nanotips, showing five distinct emission peaks from 514-635 nm/RYG. The growth parameters of the InGaN MQWs such as growth rate,[38-39] time[40-41] and temperature[42-43] are traditionally manipulated to increase the indium content and consequently increase the emission wavelength. However this increasing indium content and/or thick MQWs results in poor crystal quality layers mostly due to the large lattice mismatch and difference in thermal expansion coefficients with the GaN barriers[44], forming centres or non-radiative recombination. For our study the growth parameters were kept constant for all five MQWs with a low indium content of ~15%. The red shift in fact appears to be achieved by simply manipulating the confinement dimensions of the active regions at the top of 3D structure nanorods. We show by STEM physical characterization of the InGaN MQWs, the inverse linear relationship between the QW thicknesses in the x/y directions to the z direction (0001 growth direction) at the top of the truncated pyramidal GaN nanorods. This greatly increased growth rate occurring selectively at the rod top c-planes, allows for the site controlled RYG emission only at the nanotips.

Experimental Section

Growth of GaN nanorods by MOCVD

The initial AlN film was grown on c-plane sapphire substrates (0.10° $\pm$ **0.02**° miscut towards the m-plane) using an Aixtron close coupled showerhead 3 x 2" MOCVD reactor. As presented in our previous work a three step temperature variation recipe was used to grow the films to a thickness of 2µm in the MOCVD reactor.[45] A ~2.5 µm bulk GaN layer was grown on the AlN layer at a V/III ratio of 2400 and growth temperature of 900 ^{o}C. The GaN films patterned by nano-spheres were then placed back into the reactor for further growth. The MOCVD growth conditions for the re-deposition of GaN used (~300 nm estimated growth thickness) were the same as for the bulk base layer. The InGaN quantum wells were grown at a growth temperature of 720 ^{o}C and an estimated thickness of 2 nm and In% of 16 (calibrated recipe based on a planar growth on bulk 11-22 semi-polar GaN). The GaN quantum barriers (QBs) were grown at 850 ^{o}C at an estimated growth thickness of 5 nm. In-situ reflectance measurements were carried out using a Laytec EpiTT system to record the growth. The susceptor surface temperature was measured by a pyrometer and compared to the spot measurements using an ARGUS CCS Pyrometric Profiling System multi-channel pyrometer for more accurate representation of the surface temperature variation during growth.

Nanosphere Lithography

The spheres were synthesized by the Stöber[46] method in ethanol to a diameter of 550 ±5 nm. Before patterning a solution was made up of the silica spheres in ethanol at 10% w/v and chloroform at a ratio of 2:3 and stirred for 30 min. This mixture was then introduced to the surface of a trough of water by a glass dropper with the GaN/AlN/Al_2O_3 wafer already submerged as previously described by Oh et al.[47] The glass trough was then lowered mechanically allowing the self-assembly of the silica particles on the emerging wafer piece. To space out the silica sphere pattern a CF_4 based inductively coupled plasma (ICP) dry etch (CF_4 12 sccm, CHF_3 28 sccm, 2.5 mT, 800W ICP, 75W RF) was used. A chlorine based ICP dry etch (Cl_2 60 sccm, pressure 7.5 mT, ICP power 700 W, RF power 200 W, temperature 50 ^{o}C) was used to transfer the pattern into the underlying GaN film forming the structures using Oxford Instruments Plasmalab 100 model. The remaining silica mask after etching was removed by soaking the film in a bath of buffered oxide solution (Sigma Aldrich ammonium fluoride – hydrofluoric acid mixture) for 5 mins to ensure a silica free surface before placing the film back in the reactor.

Structural Characterisations

FEI Quanta 650 field emission gun (FEG) high resolution scanning electron microscope (SEM) was utilized to obtain a visual representation of the overgrowth surface. The crystal structure and defect analysis was characterised on all samples using a JEOL 2100 200 keV high resolution transmission electron microscope (TEM). Cross sectional TEM specimens were prepared with a focused ion beam (FIB) using a FEI HELIOS NanoLab 600 dual-beam system. Individual nanorods were scratched off onto poly-carbon mesche copper TEM grids using a handheld diamond tipped scribe. STEM and EDX mapping analysis was done in a 300keV FEI Titan STEM. CL hyperspectral imaging analysis was conducted in an environmental SEM with a 600 lines/mm grating, blazed at 200 nm, a focal length of 125mm and a 1600-element charge-coupled device. The samples were tilted by 45^{o} with respect to the incident electron beam and the generated light is collected by a reflecting objective with its optical axis perpendicular to the electron beam.

Results and Discussion

Using the same self-assembly method as in our previous report for AlN nanorods[48-49] a close packed nano dimensional silica sphere hard mask (SSHM) was coated over the entire 2" wafer, as seen in the photograph of Fig. 1e. The close packed SSHM was spaced out using an oxide ICP etch, as described in the experimental section, which selectively etched/shrunk the silica spheres without affecting the GaN bulk layer, schematically represented in Fig. 1a and b. The spaced-out pattern was then transferred into the GaN using a Cl_2 based ICP etch to form ~1.75 µm long nanorods, as seen in the illustration and SEM of Fig. 1c. An estimated 300 nm of GaN was overgrown on nanorod patterns (estimated by in-situ growth reflectance measurements carried out on a planar GaN wafer). The SEM imaging of the resulting overgrowth surface as seen below the schematic illustration in Fig. 1d, reveals the highly dense semi-polar sided pyramidal topped GaN nanorods without coalescence.

To overcome the parasitic growth and coalescing between the GaN rods, the originally etch depth was increased to a depth longer than the estimated diffusion length of the Ga adatom species under these growth parameters. Hence any GaN deposition/growth at points further down the nanorod can only occur due to the direct impingement of the incoming flux. GaN overgrowth on nanorod patterns etched for a shorter etch time of 1 min (etch depth of ~700 nm) resulted in the coalesced regions between adjacent rods as expected, as presented in ESI Fig. S1. Therefore after a certain nanorod etch depth there will be no GaN growth, keeping the adjacent nanrod bases separate and avoiding any parasitic growth between the bases of the rods.

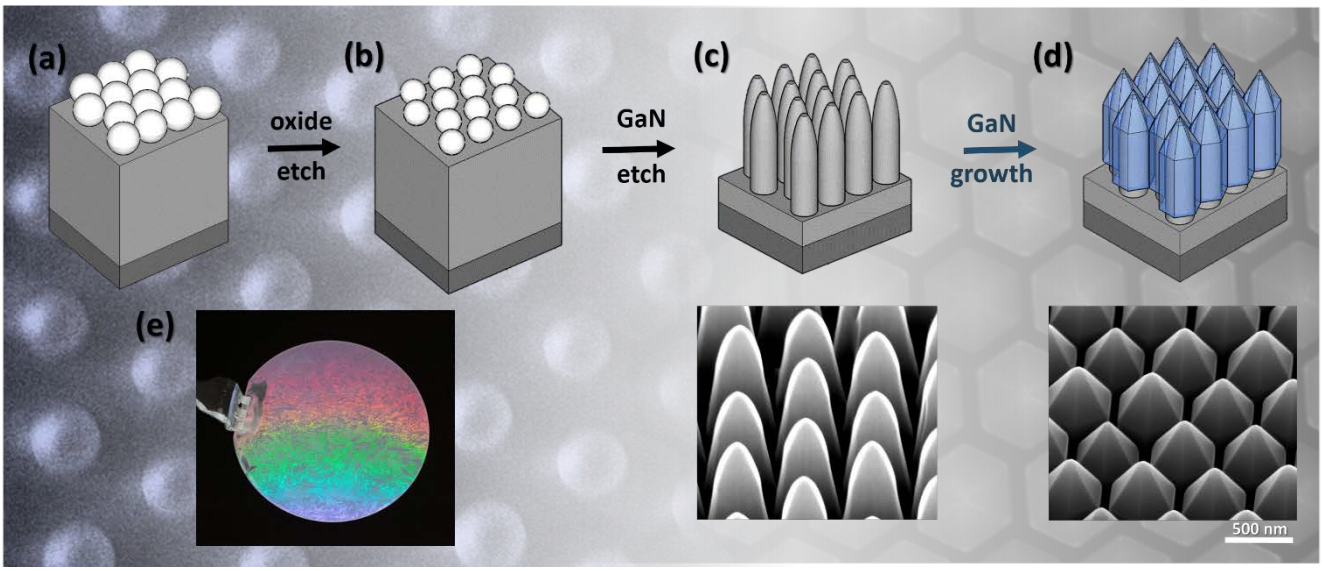

Fig. 1 Schematic illustration of the processing and growth steps of the GaN nanorod formation (a) close packed monolayer of silica spheres on GaN bulk layer, (b) spaced out monolayer pattern after oxide etch, (c) nanorods formed after 3 min Cl_2 etch, with SEM inset of the top surface, (d) 300 nm of GaN overgrowth on (c), with SEM inset revealing the apex tipped nanorods, (e) photograph of 2" GaN/AlN/Al_2O_3 wafer coated with a monolayer of silica spheres.

The naturally occurring hexagonal alignment of the top-down etched nanorod pattern resulted in a non-polar sidewall meeting point of the grown nanorods. The stability of these non-polar facets inhibited the coalescence of the rods at these meeting points under the growth conditions used, hence an ultra-dense array of space filling nanorods was easily achieved even at high temperature of 900 °C. Due to the randomness of the GaN nanorods positioning when growth is done using spontaneous growth modes[22], coalescence occurs easily and the highest space filling factor without coalescence achieved to date is only 50%.[36] The issue of coalescing is only seen for our approach when the pattern of the original silica sphere hard mask was not well aligned. Although there are many benefits to self-assembly patterning, long ranged order is only achievable to a certain extent. When the grain boundaries of two crystallites meet the change in the ordering can result in a "perfect misalignment", where one of the adjacent nanorods is twisted by 30° to the neighboring rod. These misaligned nanorods coalesce causing the vertical growth rate to increase at these points as seen in ESI Fig. S2. However, with increasing growth deposition (300 nm → 1 µm) the majority of the nanorods remain stand-alone it is still only at the "perfectly misaligned" points that coalescence occurs.

After the GaN top down/bottom up nanorods are formed, InGaN/GaN quantum well/quantum barriers (QW/QBs) are deposited using the growth condition for forming planar QWs on 11-22 semi-polar GaN in the MOCVD reactor (QB growth temperature = 850 °C and QW growth temperature = 720 °C). The estimated indium content for the InGaN MQWs grown was 16% according to growth on bulk planar semi-polar GaN. After growth a pointed pyramidal structure is formed at the top of the nanorods, as seen in Fig. 2c, with the slanted facets in the 1-101 planes, which form a tilted angle of 62° following the same geometry of the GaN nanorod core as seen in SEM analysis of Fig. 1d. The ultra-sharp tip can be seen clearly in Fig. 2d under transmission electron microcopy (TEM) imaging with the selective area electron diffraction (SAED) revealing the single crystal wurtzite structure. The lower growth temperatures of the QW/QBs promote the vertical/0001 growth rate as reported by Hiramatsu et al[50] for GaN micro-stripes, and as a result any c-plane facet at the top of these rods is shrunk to a sharp tip as seen in Fig. 2c.

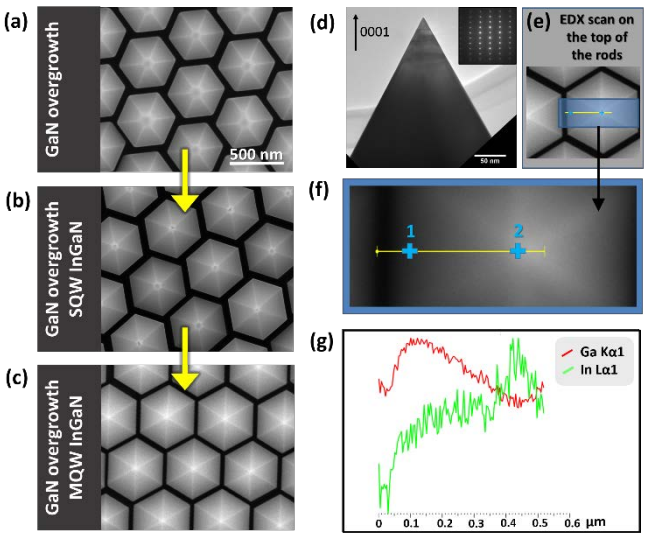

Fig.2 SEM imaging of (a) GaN nanorod overgrowth with truncated apex tips, (b) InGaN/GaN SQW growth on (a) with a smaller c-plane diameter top, (c) InGaN/GaN MQW growth on (a) with a sharp apex tip, (d) TEM of the sharp tip on an individual nanorod with SAED inset showing the wurzite crystal structure with the 0002 growth direction, (e) and (f) EDX line and point scan in SEM mode, (g) spectra from the line scan in (e) and (f).

When a single QW(SQW)/QB of InGaN/GaN is grown on the GaN nanorods, as seen in Fig. 2b, the original c-plane although shrinks in diameter, but it does not fully disappear as seen for the MQW nanrods. Reinforcing the idea of increased 0001 growth rate with decreasing growth temperature as stated above. This implies the top diameter and in turn c-plane QW diameter can be controlled easily by manipulating the growth time of the low temperature QB. Initial EDX point scans from the top surface of the nanrod, blue crosses in Fig. 2e, measured a 10 fold increase in In% at the tips compared to the semi-polar sidewalls. The line scan also shows this sharp increase of In% at the top of the nanorods with comparable decrease in Ga content as seen in Fig. 2f and g. This result alone indicated that either the indium composition of the *c*-plane MQW region was higher than the In composition at the semi polar-plane MQW region or simply the well thickness at the c-plane was far greater in thickness. However through STEM investigation as seen in Fig. 5, it was revealed that this sharp peak in In content was due to the much higher growth rate in the c-plane direction for InGaN QWs than at the semi-polar planes also observed by Tu. C.G et al[51].

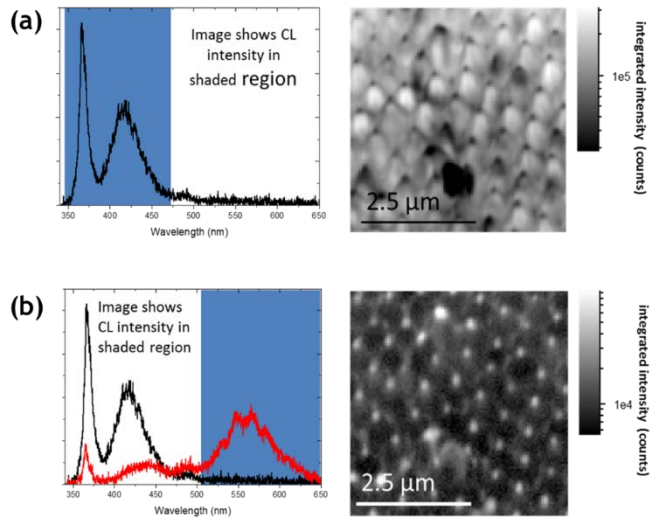

Fig. 3 Correlative CL spectra and SEM imaging of the emission: (a) ~350-450 nm spectral range from the semi-polar sidewalls and (b) >500 nm spectral range from only the nanotips.

The initial CL measurements of the close packed nanorod arrays shows the blue emission is coming from the semi-polar planes and not from the nanotips as seen in the emission spectrum highlighted in blue in Fig. 3a. The tips of each nanorod however emit light in the visible light spectrum >500 nm (highlighted blue region in Fig. 3(b)), with no emission in the spectral range coming from the rest of the nanorod. The Correlative CL and SEM of Fig. 3b reveal the drastically different emission wavelength at the tips. This result is in positive agreement with the EDX top surface line scans as seen in Fig. 2g. The room temperature photoluminescence analysis in Fig. S3 of ESI of the rods reveals a broad peak in the same wavelength region (i.e. red, yellow, green) as seen for the highlighted red CL spectra of Fig. 3b. To investigate the nanoscale optical properties at the nanorod tip and the source of the possible change in composition/well thickness nanorods were exfoliated from the bulk substrate. This was done by using a diamond scribe to scratch off the rods and then dropping onto a lacey poly carbon covered copper grid for scanning transmission electron microscopy (STEM) and CL hyperspectral imaging, Fig. 4 and 5.

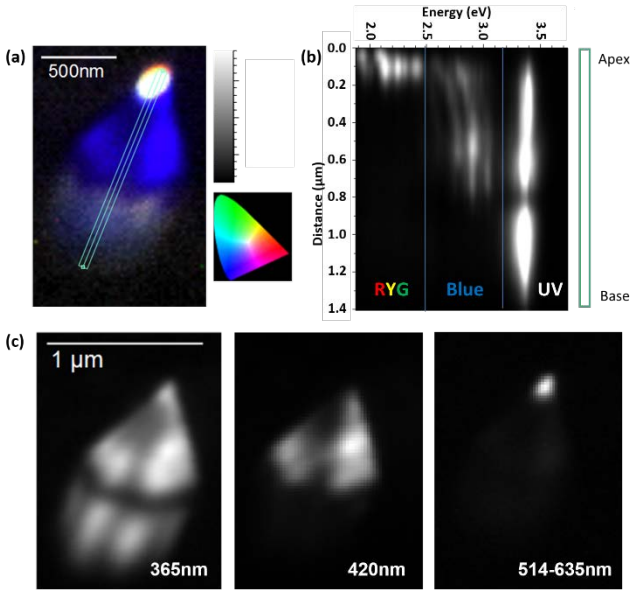

Fig. 4 (a) real colour representation of the spatially resolved CL emission, (b) spectral information extracted along the line in (a), (c) spatially resolved CL of the nanorod at increasing wavelength range.

The real colour representation of the spatially resolved CL emission in Fig. 4a, shows the white light emission from the nanotips. Extracting the spectral information along the line in Fig. 4a gives a line spectrum with three distinctive regions of the nanorod of different optical properties; non-polar sidewalls, semi-polar sidewalls and the c-plane tip, as seen in Fig. 4b. What is noticeable in the non-polar region is the lack of any yellow luminescence and the small FWHM of the 365 nm peak (Fig. 3a), indicating any possible ion beam damage incorporated during the etched nanorod formation was healed. This links well with our previous report for AlN[49] on dislocation reduction of III-N etched nanorods after thermal annealing at MOCVD growth temperatures, that will also be discussed in a detailed report on GaN nanorod annealing in a future publication. The intensity map in this UV region (Fig. 4c ~365 nm) shows a strong reduction in the luminescence intensity at the point where the top and base of the nanorod meet.

The second region at the semi-polar sidewalls is dominated by a broad luminescence band in the blue region (395-465 nm). In the line spectrum there is one main peak with two satellite peaks. It has been suggested that these three peaks may be due to the influence of optical modes within the rod since the growth conditions for the 5 InGaN MQWs were not varied throughout the growth. Kusch et al will report this CL analysis in a future publication.

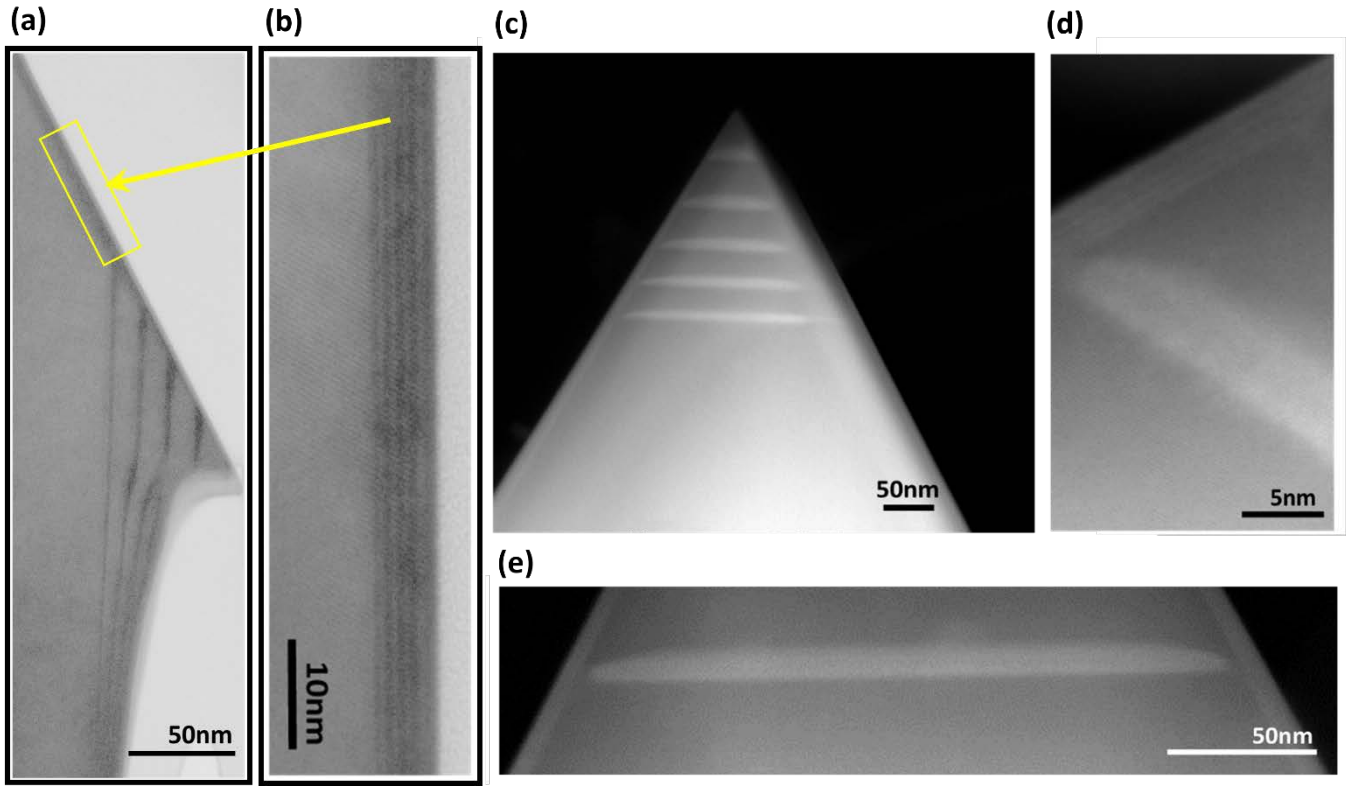

Fig. 5 TEM imaging of (a) the semi-/non-polar meeting point revealing the changing in MQW thickness, (b) higher magnification of the 5 X MQWs on the semi-polar facets, STEM imaging of (c) the nanorod tip showing the 5 X MQWs increasing in thickness, (d) higher magnification of the meeting point of the 5 X MQWs visible at the semi-polar facet to the first c-plane QW, (e) lower magnification showing the first c-plane QW thickness is greater than the entire 5 X MQW/MQB at the semi-polar plane.

The third light emitting region seen in Fig. 4b from the nanotip exhibits a broad luminescence band consisting of multiple peaks covering the visible spectral range from green to red (514-635 nm). TEM/STEM analysis of the nanorod tip, shown in Fig. 5, show a c-plane MQW structure at the apex of the nanorod, consisting of 5 QWs. This finding strongly suggests that these QWs are the origin of the luminescence band from the apex of the nanorod.

FIB cross sections of the ~550 nm thick nanorods were done to analyze under a 200keV TEM in high resolution as in Fig. 5a and b. The stacked bright and dark layers, corresponding to the InGaN QW and QB respectively. Fig. 5a shows the edge between the non-polar (1-100) and semi-polar (1-101) planes which reveals slightly thicker QW width, other groups have explained this by possible different incorporation rates at the edge region due to gas flow i.e. flux shielding of the non-polar plane[52]. However unlike at the thicker QWs on the c-plane where there is a clear individually sharp luminescence peaks (RYG) seen in CL, these meeting points of the non- and semi-polar planes results in nearly no luminescence under CL investigation as seen in Fig. 4b and c. This suggests that the irregularity of the QWs at this meeting point as seen in the TEM image of Fig. 5a suppresses the luminescence. The TEM/STEM clearly show significantly large differences in the QW and QB thickness on different growth facets, which may be a result of the anisotropic surface formation energies of GaN crystal planes that are known to influence the diffusion of adatoms.[15, 53-54] The nanorods scratched off for the CL analysis were investigated by STEM as shown in Fig. 5d-e. This analysis shows the thickest active region growth area (i.e. fastest growth direction) is in the c-plane/0001 growth direction. The decreasing width of the c-plane with increasing growth thickness produces a MQW geometry more like that of multiple quantum discs (MQDs).

Analysis by surface area spectra done in Image J software illustrates and measures by a 3D model the increasing thickness of the QDs and QBs going up the nanorod. Fig. 6a is the 3D spectra along the area indicated with the yellow arrow in the STEM EDX spectra image in Fig. 6b, used to extract the lengths of the QDs and QBs. When plotted against each other the increasing QD/QB thickness is seen to have a near linear relationship, Fig. 6c. This is a clear indication that the increasing InGaN QD thickness is not principally due to the higher indium adatom diffusion length that has been an argument for thicker c-plane active region and higher In % incorporations.[14] Instead the linear relationship with the GaN barrier indicates the change in the QD thickness is thus a direct result in increased growth rate due to the decreasing x/y directional geometry as schematically illustrated in Fig. 6e. The 5 luminescence peaks at 516, 534, 551, 577, and 635 nm corresponding to the RYG

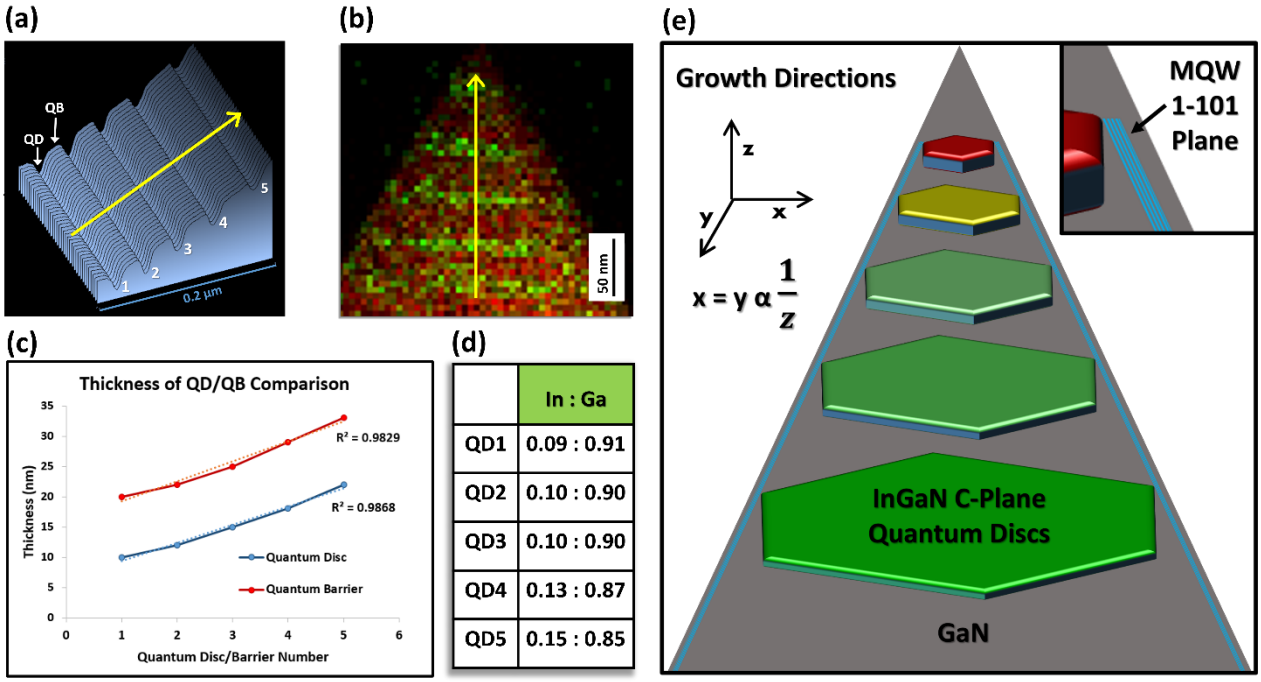

Fig. 6 (a) Surface area plot of the 5 X MQD/QBs along the yellow line of (b) the edx mapping of the 5 MQDs, graphical plot of the QD/QW thickness data obtained from (a), (d) table of the In : Ga wt% rato data at each MQD, (e) schematic illustration of the changing thickness for the InGaN wells in all three x,y,z directions at the c-plane.

luminescence clearly distinguishable in Fig. 4 and the spectra of ESI Fig. S4. This can be compared to the drastically changing confinement seen in Fig. 5 STEM imaging and schematically represented in Fig. 6e. The x/y:z ratio of the InGaN QWs change from 18:1 for the first QW to 1.5:1 for the fifth and final QW, numerically portraying the profound shift in directional confinement along the pyramid top.

EDX mapping in STEM high angle annular dark field (HAADF) mode was undertaken at 300 keV to investigate the elemental compositional ratios of the InGaN active regions, Fig. 6b. There was an increase in the In% as detailed in the table of Fig. 6d from QW1 (9%) to QW5 (15%), however this increase in In% may not be this high in reality when taking into account the possible errors due to the change in interaction volume at the 3D structure of the nanotip. Even with this observed increase in In% the corresponding InGaN alloy ratio is still far too low to emit light in the RYG region of the visible light spectrum, when compared to theoretical calculations and experimental c-plane bulk InGaN QW reports.[55] However Liao. C.H. et al[56] show a much lower In% is needed in InGaN QWs nanorods (15.6-16.8%) for emission >500 nm when the thickness of the wells is increased ~22 nm that is identical to the thickness in the z-direction for our c-plane QWs as seen in Fig. 6c. As described above the growth of these very thick InGaN layers occurred only at the c-plane due to an increased growth rate with the decreasing x/y directional geometry hence the red shift in emission is only seen on the tips of the nanorods and not in the 2 nm thick semi-polar wells.

A possible application for these nanorod geometries would be to concentrate on the growth of single InGaN QDs on the top of these nanorods for single photon emission. The growth of such QDs has been demonstrated via the Stranski-Krastanov growth mode[57] and other routes.[58] However, these methods do not allow the control of the position and even the size of the nanostructures, which is an essential requirement for applications such as single photon emitters.[59] This growth method of InGaN/GaN nanorods provides a template to allow for wafer-scale position controlled growth of InGaN QD arrays as demonstrated by Juska et al[60] for InGaAs QDs grown in inverted pyramidal arrays.

Conclusion

The results presented in this article prove an emission wavelength >600 nm can be achieved simply by manipulating the directional confinement of InGaN films without increasing the indium of the InGaN MQWs to a high molar fraction. With the stable m-plane nanorod sidewalls formed, the c-plane diameter decreases with the increasing z height following the stabilized 62° semi-polar sidewall along this naturally occurring 1-101 plane. Hence we see an increase in growth rate of both the InGaN MQWs and the GaN barriers without any change in the applied growth parameters within the MOCVD reactor. Therefore along with the experimentally measured low In%, the possible explanation of compositional pulling often suggested to explain changes in QW thickness on different growth facets and thus shifts in the expected emission wavelength can be eliminated. We conclude that the red shift is most likely due to the considerable change in directional confinement at the nanotips, resulting in thick (>20 nm) InGaN QDs rather than a QW geometry.

TEM and STEM show the dislocation and stacking fault free nature of the nanorods and active regions, revealing the high crystalline quality of these highly dense wafer scale arrays of non-coalesced InGaN/GaN nanorods. The results of this article put forward many possible applications for these nanorods including broad spectrum white lighting sources, but more interestingly possible single photon emitting light sources across the visible light spectrum with controlled positioning of the InGaN QDs on these ordered highly dense nanorod arrays.

Acknowledgements

This research was enabled by the Irish Higher Education Authority Programme for Research in Third Level Institutions Cycles 4 and 5 via the INSPIRE and TYFFANI projects, and by Science Foundation Ireland (SFI) under Grant no. SFI/10/IN.1/I2993. PJP acknowledges funding from SFI Engineering Professorship scheme (07/EN/E001A) and MC acknowledges PhD research scholarship from INSPIRE. This work was conducted under the framework of the Irish Government's Programme for Research in Third Level Institutions Cycle 5, National Development Plan 2007–2013 with the assistance of the European Regional Development Fund. RWM and GK acknowledge funding from the Engineering and Physical Sciences Research Council (EPSRC) (EP/M003132/1) of the UK. We also acknowledge the support of Duc V. Dinh for his help with the PL spectra and William Jagoe for his illustrations in the article.

References

1 D. F. Feezell, J. S. Speck, S. P. DenBaars, and S. Nakamura, *Journal of Display Technology*, 2013, **9**, 190-198.
2 J. Herrnsdorf, J. J. D. McKendry, Z. Shuailong, X. Enyuan, R. Ferreira, D. Massoubre, A. M. Zuhdi, R. K. Henderson, I. Underwood, S. Watson, A. W. Kelly, E. Gu, M. D. Dawson, *IEEE Transactions on Electron Devices*, 2015, **62**, 1918-1925.
3 H. X. Jiang and J. Y., Lin, *Opt. Express* 2013, **21**, 475-484.
4 J. Wu, W. Walukiewicz, K. M. Yu, J. W. Ager, E. E. Haller, H. Lu, and J. W. Schaff, *Appl. Phys. Lett.,* 2002, **80**, 4741-4743.
5 J. H. Kim, Y. H. Ko, J. H. Cho, S. H. Gong, S. M. Ko, and Y. H. Cho, Nanoscale 2014, **6**, 14213-14220.
6 T. Detchprohm, M. Zhu, Y. Li, L. Zhao, S. You, C. Wetzel, E. A. Preble, T. Paskova, and D. Hanser, Appl. Phys. Lett. 2010, **96**, 051101.
7 W. Zhao, L. Wang, J. Wang, Z. Hao, and Y. Luo, *J. Cryst. Growth*, 2011, **327**, 202-204.
8 R. People and J. C. Bean, *Appl. Phys. Lett.*, 1985, **47**, 322-324.
9 K. Nakajima, T. Ujihara, S. Miyashita and G. Sazaki, *J. Appl. Phys.*, 2001, **89**, 146-153.
10 S. D. Hersee, X. Sun and X. Wang, *Nano Lett*., 2006, **6**, 1808-1811.
11 M. E. Coltrin, A. M. Armstrong, I. Brener, W. W. Chow, M. H. Crawford, A. J. Fischer, D. F. Kelley, D. D. Koleske, L. J. Lauhon, J. E. Martin, M. Nyman, E. F. Schubert, L. E. Shea-Rohwer, G. Subramania, J. Y. Tsao, G. T. Wang, J. J. Wierer, J. B. Wright, *J. Phys. Chem. C*, 2014, **118**, 13330-13345.
12 W. Guo, M. Zhang, A. Banerjee and P. Bhattacharya, *Nano Lett.*, 2010, **10**, 3355-3359.
13 J. W. Jonathan, L. Qiming, D. K. Daniel, R. L. Stephen and T. W. George, *Nanotechnology*, 2012, **23**, 194007.
14 T. W. Yeh, Y. T. Lin, L. S. Stewart, P. D. Dapkus, R. Sarkissian, J. D. O'Brien, B. Ahn and S. R. Nutt, *Nano Lett.*, 2012, **12**, 3257-3262.
15 Y. J. Hong, C.H. Lee, A. Yoon, M. Kim, H. K. Seong, H. J. Chung, C. Sone, Y. J. Park and G. C. Yi, *Adv. Mater.,* 2011, **23**, 3284-3288.
16 R. Yan, D. Gargas and P. Yang, Nat Photon 2009, **3**, 569-576.
17 Y. H. Ko, J. H. Kim, S. H. Gong, J. Kim, T. Kim, and Y. H. Cho, *ACS Photonics*, 2015, **2**, 515-520.
18 J. B. Wright, S. Liu, G. T. Wang, Q. Li, A. Benz, D. D. Koleske, P. Lu, H. Xu, L. Lester, T. S. Luk, I. Brener and G. Subramania, Multi-Colour Nanowire Photonic Crystal Laser Pixels. *Sci. Rep.* 2013, **3**.
19 C. Park, Y. Park, H. Im and T. Kang, *Nanotechnology*, 2006, **17**, 952.
20 X. Duan and C. M. Lieber, J. Am. Chem. Soc. 2000, **122**, 188-189.
21 T. Kuykendall, P. Pauzauskie, S. Lee, Y. Zhang, J. Goldberger and P. Yang, *Nano Lett.*, 2003, **3**, 1063-1066.
22 O. Brandt, S. Fernández-Garrido, J. K. Zettler, E. Luna, U. Jahn, C. Chèze and V. M. Kaganer, Cryst. Growth Des., 2014, **14**, 2246-2253.
23 B. Jenichen, O. Brandt, C. Pfüller, P. Dogan, M. Knelangen and A. Trampert, *Nanotechnology*, 2011, **22**, 295714.
24 S. Fan, S. Zhao, X. Liu, Z. Mi, *J. Vac. Sci. Technol., B*, 2014, **32**, 02C114.
25 V. Consonni, M. Knelangen, U. Jahn, A. Trampert, L. Geelhaar and H. Riechert, *Appl. Phys. Lett.*, 2009, **95**, 241910.
26 P. Lefebvre, S. Fernández-Garrido, J. Grandal, Ristić, J.; Sánchez-García, M.-A.; Calleja, E., Radiative defects in GaN nanocolumns: Correlation with growth conditions and sample morphology. *Appl. Phys. Lett.*, 2011, **98**, 083104.
27 S. Fernández-Garrido, V. M. Kaganer, C. Hauswald, B. Jenichen, M. Ramsteiner, V. Consonni, L. Geelhaar and O. Brandt, *Nanotechnology*, 2014, **25**, 455702.
28 L. Yan, S. Jahangir, S. A. Wight, B. Nikoobakht, P. Bhattacharya and J. M. Millunchick, *Nano Lett.*, 2015, **15**, 1535-1539.
29 O. Brandt, C. Pfüller, C. Chèze, L. Geelhaar and H. Riechert, *Phys. Rev. B: Condens. Matter*, 2010, **81**, 045302.
30 M. A. Reshchikov and H. Morkoç, Luminescence properties of defects in GaN. *J. Appl. Phys.*, 2005, **97**, 061301.
31 J. H. Kim, C. S. Oh, Y. H. Ko, S. M. Ko, K. Y. Park, M. Jeong, J. Y. Lee and Y. H. Cho, *Cryst. Growth Des.*, 2012, **12**, 1292-1298.
32 Q. Li, J. B. Wright, W. W. Chow, T. S. Luk, I. Brener, L. F. Lester and G. T. Wang, *Opt. Express*, 2012, **20**, 17873.
33 Q. Li, K. R. Westlake, M. H. Crawford, S. R. Lee, D. D. Koleske, J. J. Figiel, K. C. Cross, S. Fathololoumi, Z. Mi and G. T. Wang, *Opt. Express*, 2011, **19**, 25528-25534.
34 J. J. Wierer, Q. Li, D. D. Koleske, S. R. Lee, G. T. Wang, *Nanotechnology*, 2012, **23**, 194007.
35 C. J. Lewins, E. D. Le Boulbar, S. M. Lis, P. R. Edwards, R. W. Martin, P. A. Shields and D. W. E. Allsopp, *J. Appl. Phys.*, 2014, **116**, 044305.
36 A. Waag, X. Wang, S. Fündling, J. Ledig, M. Erenburg, R. Neumann, M. Al Suleiman, S. Merzsch, J. Wei, S. Li, H. H. Wehmann, W. Bergbauer, M. Straßburg, A. Trampert, U. Jahn and H. Riechert, *Phys. Status Solidi C*, 2011, **8**, 2296-2301.
37 M. Conroy, V. Z. Zubialevich, H. Li, N. Petkov, S. O'Donoghue, J. D. Holmes and P. J. Parbrook, *ACS Nano*, 2015.
38 T. Matsuoka, N. Yoshimoto, T. Sasaki and A. Katsui, *J. Electron. Mater.*, 1992, **21**, 157-163.
39 S. Keller, B. P. Keller, D. Kapolnek, A. C. Abare, H. Masui, L. A. Coldren, U. K. Mishra, S. P. Den Baars, Growth and characterization of bulk InGaN films and quantum wells. *Appl. Phys. Lett.*, 1996, **68**, 3147-3149.
40 S. F. Chichibu, A. C. Abare, M. P. Mack, M. S. Minsky, T. Deguchi, D. Cohen, P. Kozodoy, S. B. Fleischer, S. Keller, J. S. Speck, J. E. Bowers, E. Hu, U. K. Mishra, L. A. Coldren, S. P.

DenBaars, K. Wada, T. Sota and S. Nakamura, *Mater. Sci. Eng., B*, 1999, **59**, 298-306.
41 D. Benjamin, G. Nicolas, P. Cyril and M. Jean, *Jpn. J. Appl. Phys.*, 2001, **40**, 918.
42 H. C. Lin, C. K. Shu, J. Ou, Y. C. Pan, W. K. Chen, W. H., Chen and M. C. Lee, *J. Cryst. Growth*, 1998, **57**, 189–190.
43 W. Van der Stricht, I. Moerman, P. Demeester, J. A. Crawley and E. J. Thrush, *J. Cryst. Growth*, 1997, **170**, 344-348.
44 F. K. Yam and Z. Hassan, Superlattices Microstruct., 2008, **43**, 1-23.
45 H. Li, T. C. Sadler and P. J. Parbrook, *J. Cryst. Growth*, 2013, **383**, 72-78.
46 W. Stöber, A. Fink and E. Bohn, *J. Colloid Interface Sci.*, 1968, 26, 62-69.
47 J. R. Oh, J. H. Moon, S. Yoon, C. R. Park and Y. R. Do, J. Mater. Chem. 2011, **21**, 14167-14172.
48 M. A. Conroy, N. Petkov, H. N. Li, T. C. Sadler, V. Zubialevich, J. D. Holmes and P. J. Parbrook, *ECS Transactions*, 2013, **53**, 39-42.
49 M. Conroy, V. Z. Zubialevich, H. Li, N. Petkov, N.; J. D. Holmes, P. J. Parbrook, J. Mater. Chem. C, 2015, **3**, 431-437.
50 K. Hiramatsu, *J. Phys.: Condens. Matter,* 2001, **13**, 6961.
51 C. G. Tu, C. Y. Su, C. H. Liao, C. Hsieh, Y. F. Yao, H. T. Chen, C. H. Lin, H. S. Chen, Y. W. Kiang and C. C. Yang, Superlattices Microstruct., 2015, **83**, 329-341.
52 B. O. Jung, S. Y. Bae, S. Y. Kim, S. Lee, J. Y. Lee, D. S. Lee, Kato, Y. Honda and H. Amano, *Nano Energy* 2015, **11**, 294-303.
53 M. Funato, T. Kotani, T. Kondou, Y. Kawakami, Y. Narukawa and T.Mukai, *Appl. Phys. Let.* 2006, **88**, 261920.
54 Y. J. Hong, S. J. A., H.S. Jung, C. H. Lee, G. C. Yi, Adv. Mater. 2007, **19** (4416).
55 N. Shuji, S. Masayuki, I. Naruhito and N. Shinichi, Jpn. J. Appl. Phys., 1995, **34**, L797.
56 C. H. Liao, C. G. Tu, W. M. Chang, C. Y. Su, P. Y. Shih, H. T. Chen, Y. F. Yao, C. Hsieh, H. S. Chen, C. H. Lin, C. K. Yu, Y. W. Kiang and C. C. Yang, *Opt. Express*, 2014, **22**, 17303-17319.
57 Y. Kobayashi, V. Perez-Solorzano, J. Off, B. Kuhn, H. Gräbeldinger, H. Schweizer, F. Scholz, *J. Crystal Growth*, 2002, **243**, 103-107.
58 T. Ru-Chin, T. Chun-Ju, C. Chang-Cheng, L. Bing-Chi, T. Ching-En, W. Te-Chung, C. Jim, L. Chien-Ping and C. Gou-Chung, Jpn. J. Appl. Phys., 2004, **43**, L264.
59 V. Pérez-Solórzano, A. Gröning, M. Jetter, T Riemann and J. Christen, Appl. Phys. Lett. 2005, **87**, 163121.
60 G. Juska, V. Dimastrodonato, L. O. Mereni, A. Gocalinska, E. Pelucchi, *Nat Photon*, 2013, **7**, 527-531.

